Ratchet Effects in Active Matter Systems

C.J. Olson Reichhardt and C. Reichhardt

Theoretical Division, Los Alamos National Laboratory, Los Alamos, New Mexico 87545; email: cjrx@lanl.gov, reichhardt@lanl.gov

Abstract

Ratchet effects can arise for single or collectively interacting Brownian particles on an asymmetric substrate when a net dc transport is produced by an externally applied ac driving force or by periodically flashing the substrate. Recently, a new class of active ratchet systems that do not require the application of external driving has been realized through the use of active matter; they are self-propelled units that can be biological or nonbiological in nature. When active materials such as swimming bacteria interact with an asymmetric substrate, a net dc directed motion can arise even without external driving, opening a wealth of possibilities such as sorting, cargo transport, or micromachine construction. We review the current status of active matter ratchets for swimming bacteria, cells, active colloids, and swarming models, focusing on the role of particle-substrate interactions. We describe ratchet reversals produced by collective effects and the use of active ratchets to transport passive particles. We discuss future directions including deformable substrates or particles, the role of different swimming modes, varied particle–particle interactions, and nondissipative effects.

1. INTRODUCTION

When a particle is placed in a symmetric periodic potential and subjected to an ac drive, in general the particle simply rocks back and forth and undergoes no net dc motion. If an external dc drive $\mathbf{F}^{dc}$ is imposed on a particle in a substrate, the particle has no net dc motion and remains pinned as long as $\mathbf{F}^{dc} < \mathbf{F}_c$, where $\mathbf{F}_c$ is the critical depinning force for motion over the substrate. Once $\mathbf{F}^{dc} > \mathbf{F}_c$, the particle enters a sliding state (1). When the motion of the particle is overdamped, its dynamics can be described by the following equation of motion:

$$\eta \frac{d\mathbf{R}}{dt} = \mathbf{F}^s + \mathbf{F}_n + \mathbf{F}_{ext} + \mathbf{F}^T, \tag{1}$$

where η is the damping constant, $\mathbf{R}$ is the position of the particle, $\mathbf{F}^s$ is the force from the substrate, $\mathbf{F}_n$ is the interaction force from the other particles, $\mathbf{F}_{ext}$ is an externally applied driving force, and $\mathbf{F}^T$ is a stochastic force representing thermal fluctuations.

The situation changes if the substrate is asymmetric. An example of a one-dimensional (1D) asymmetric substrate potential with periodicity a,

$$U(x) = U_0[\sin(2\pi x/a) + 0.25 \sin(4\pi x/a)], \tag{2}$$

is illustrated in **Figure 1a**. In the absence of thermal fluctuations, the maximum pinning force exerted by the substrate on the particle for motion in the positive x direction is $3\pi U_0/a$, whereas the maximum pinning force for motion in the negative x direction has a smaller value of $3\pi U_0/2a$. As a result, if an externally applied ac driving force of the form $\mathbf{F}_{ext} = \mathbf{F}^{ac} \cos(\omega t)\hat{\mathbf{x}}$ is introduced, then the particle remains trapped and oscillates within a single potential minimum for $\mathbf{F}^{ac} < 3\pi U_0/2a$. In contrast, when $3\pi U_0/a \leq \mathbf{F}^{ac} < 3\pi U_0/2a$, the particle can overcome the substrate potential barrier for motion in the negative x direction but cannot overcome the barrier for motion in the positive x direction, so that during each ac cycle the particle undergoes a net dc transport in the negative x direction. Such motion is termed a ratchet effect. The amount of dc translation, or transport flux, that occurs per cycle depends on the amplitude and frequency of the ac drive. For fixed ac frequency, the transport flux of the ratchet is generally nonmonotonic, increasing with increasing $\mathbf{F}^{ac}$ for $\mathbf{F}^{ac} < 3\pi U_0/2a$ and then decreasing with increasing $\mathbf{F}^{ac}$ at higher $\mathbf{F}^{ac}$ (2).

When the mechanism responsible for producing a ratchet effect is an ac driving force, the system is known as a rocking ratchet. An alternative mechanism operates in a flashing ratchet, in which thermally diffusing particles are placed on a substrate that is periodically flashed on and off, and a maximum ratchet efficiency emerges as a function of flashing frequency (2). In the single-particle limit for overdamped particles, the ratchet effect causes the particle to translate along the easy direction of the substrate regardless of the nature of the ratchet. When collective particle–particle interactions are introduced, however, it is possible to observe reversals of the ratchet effect, in which the motion is along the hard direction of the substrate asymmetry (2–5). These reversals are often produced by commensurability effects between the interacting particles and the substrate, in which emergent quasiparticle objects such as kinks or antikinks dominate the transport and behave as if they are moving through an inverted substrate potential. Examples of higher-dimensional asymmetric substrates on which ratchet effects can occur appear in **Figure 1b**, which shows a quasi-1D asymmetric potential with no structure transverse to the asymmetry direction (5, 6), and in **Figure 1c**, which shows a linear array of V-shaped barriers (7). The asymmetry necessary for generating ratchet effects can also be introduced by placing individual symmetric pinning sites in an array that has a density gradient along one direction (8). In geometric or drift ratchets, which require a minimum of two spatial dimensions, particles driven over an asymmetric substrate by a dc drive undergo a net dc drift in the direction transverse to the applied dc drive (9–11). In transverse ratchets, which are a variation of drift ratchets, a net dc ratchet motion arises in the
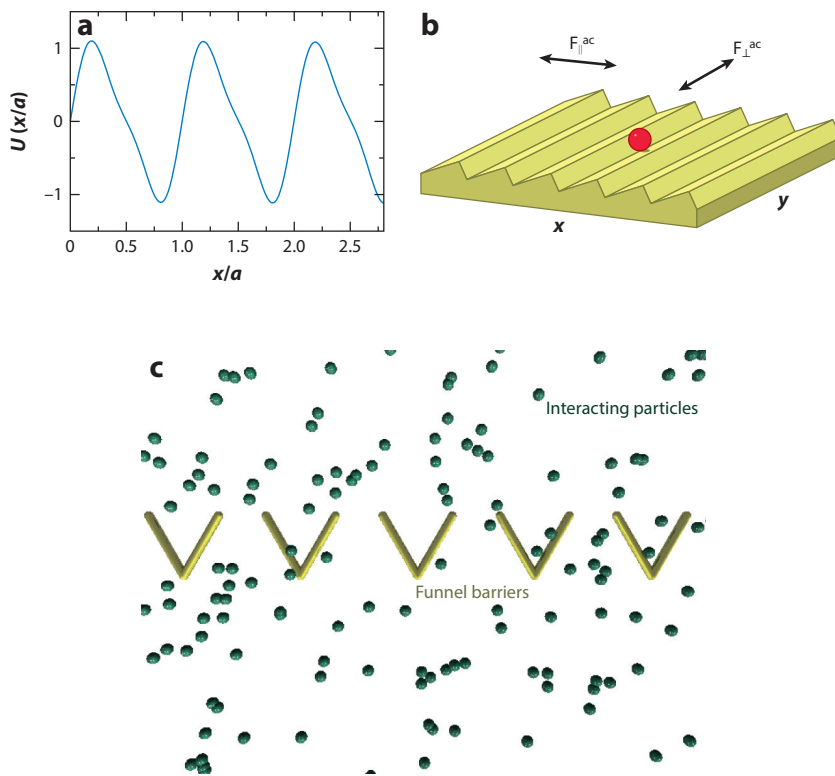
Figure 1

(*a*) A plot of an asymmetric one-dimensional (1D) substrate potential. Under an ac drive, the ratcheting motion of particles is in the easy direction of the substrate, corresponding to the negative *x* direction. (*b*) A quasi-1D version of the same substrate for particles moving in two dimensions. Adapted from Reference 16 with permission (**http://iopscience.iop.org/article/10.1088/1367-2630/17/7/073034**). (*c*) A line of 2D funnels or barriers (*yellow*) affecting the motion of interacting particles (*green*). The easy direction for the ratchet effect is the positive *y* direction, toward the top of the panel.

direction transverse to an applied ac driving force (12–14). Additional ratchet effects, including ratchet reversals, can arise when there are nondissipative terms in the equations of particle motion, such as inertia (15) or a Magnus term (16).

Studies of ratchet effects have been performed for colloids interacting with asymmetric flashing substrates (17), vortices in type-II superconductors interacting with asymmetric periodic 1D (5, 6) and 2D substrates (4, 12–14), granular matter on sawtooth substrates (18, 19), cold atoms (20, 21), electron systems (22, 23), and domain walls moving over asymmetric substrates (24, 25). These systems require the application of some form of external driving to create the nonequilibrium conditions necessary for a ratchet effect to occur.

In a different class of nonequilibrium systems, the dynamics is governed by internal driving or self-propulsion (26–29). These active matter systems include flocking and swarming particles, pedestrian and traffic flow, swimming bacteria, crawling cells, and actin filaments. Active matter is attracting attention owing to the increasing availability of nonbiological active systems such as artificial swimmers, self-driven colloids, robot swarms, and autonomous agents. Such systems exhibit a variety of phenomena, including pattern formation (30), self-clustering (31–34), and nonequilibrium phase transitions (35), and represent a rich and very active field of research. In

this review, we focus on ratchet effects in this new class of active matter systems. The review is organized as follows: In Section 2, we describe ratchet effects that arise for active matter placed in funnel arrays or similar asymmetric geometries, where the active particles can be bacteria, artificial swimmers, eukaryotic cells, or swimming animals. In Section 3, we describe additional effects that can arise in active matter assemblies where particle–particle interactions play an important role. These effects include ratchet reversals and the transport of passive particles by active particles. In Section 4, we consider ratchet effects for circle swimmers where chirality is important, whereas in Section 5, we briefly describe the ratchet-induced transport behavior that can arise when the active particles interact with an asymmetric substrate that can respond dynamically to their motion.

2. RATCHET EFFECTS FOR SWIMMERS IN FUNNEL ARRAYS

One of the first demonstrations of an active matter ratchet was achieved by P. Galajda et al. (7) for a system of *Escherichia coli* swimming in a sample divided into two chambers by an array of funnel-shaped barriers similar to those illustrated in **Figure 1c**. The entire sample is 400 μm on a side, whereas the funnel barriers, each 27 μm long, form a 60° angle at their tips and have a minimum separation of 3.8 μm between adjacent funnels. If Brownian particles are placed at a uniform density in such a geometry, the density remains equal in both chambers of the sample. In contrast, when an equal number of swimming bacteria are introduced into each chamber, after roughly an hour there is a buildup of bacteria in the chamber that is on the easy-flow side of the funnel barriers, as illustrated in **Figure 2a,b**. In the figure, the easy flow direction is to the right. In **Figure 2c**, the ratio A of the bacterial concentration ρ in the right and left chambers, $A(t) = \rho_R(t)/\rho_L(t)$, has an initial value of $A = 1.0$ at time $t = 0$ and saturates to a value of $A = 3.0$ at longer times, showing that a ratchet effect is occurring. When the same experiment is performed with chambers separated by symmetric holes instead of asymmetric funnels, then $A(t) = 1.0$ at all times, indicating that the asymmetry of the funnel is a crucial ingredient for the occurrence of rectification. When a mixture of swimming and nonswimming bacteria is placed in the sample,
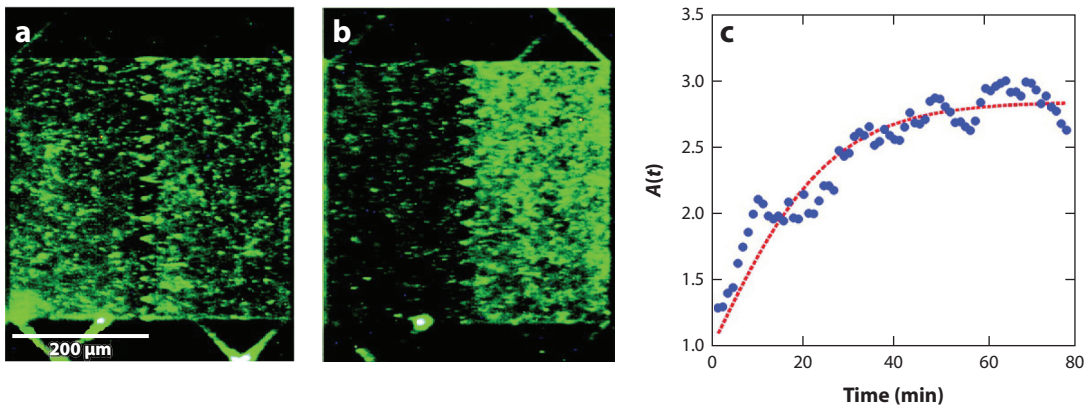
Figure 2

(a,b) Experimental images of the concentration of bacteria, indicated by fluorescence, in two chambers separated by a series of funnel barriers resembling those illustrated in **Figure 1c**. The easy flow direction through the barriers is toward the right chamber. (a) The initial uniform distribution of bacteria at time $t = 0$. (b) The distribution at $t = 80$ min, showing that the bacteria concentration is significantly higher in the right chamber. (c) The ratio $A = \rho_R/\rho_L$ of the bacteria density ρ in the right and left chambers versus time, showing that a rectification effect is occurring. Reproduced from Reference 7 with permission, ©2007 by the American Society for Microbiology.
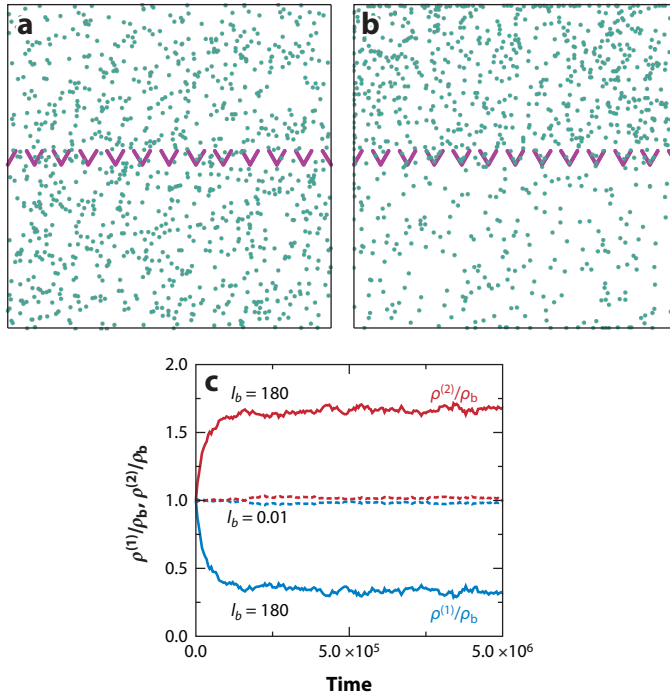
Figure 3

(*a,b*) Simulation images of noninteracting run-and-tumble particles moving between two chambers separated by a line of funnel-shaped barriers. The easy flow direction of motion through the funnels is toward the top chamber. A particle striking a funnel or chamber wall runs along the wall until reaching the end of the wall or undergoing a tumbling event. (*a*) The initial uniformly dense condition for particles with a run length of $l_b = 40$ between tumbles. (*b*) After 100 tumbling events, the particle density in the upper chamber has increased. (*c*) Ratios $\rho^{(1)}/\rho_b$ (*red line*) and $\rho^{(2)}/\rho_b$ (*blue line*) of the particle density $\rho^{(1)}$ in the upper chamber and $\rho^{(2)}$ in the lower chamber, respectively, to the initial particle density ρ_b as a function of time. Solid lines are for a sample with a run length of $l_b = 180$ in which there is a large rectification effect, and dashed lines are for a sample with a run length of $l_b = 0.01$ in which the rectification effect is negligible. Adapted from Reference 36 with permission, ©2008 by the American Physical Society.

the swimming bacteria are rectified, whereas the nonswimming bacteria are not, showing that swimming is also important in producing the ratchet effect. Due to the complexity of bacterial systems, it was not obvious whether this initial observation of an active matter ratchet effect was produced solely by the dynamics of self-propulsion combined with bacteria–wall interactions or whether more complex bacterial behaviors play a role in the ratcheting motion.

Wan et al. (36) subsequently studied a simple model of point-like run-and-tumble particles moving in a 2D container with the same funnel-barrier geometry used in the experiments of Reference 7, as illustrated in **Figure 3**. In this model, particle i obeys the following overdamped equation of motion,

$$\eta \frac{d\mathbf{R}_i}{dt} = \mathbf{F}_i^m(t) + \mathbf{F}_i^T + \mathbf{F}_i^B + \mathbf{F}_i^S, \qquad (3)$$

where η is the damping coefficient and $\mathbf{R}_i$ is the location of particle i. Instead of the external driving force used in Equation 1, Equation 3 contains a motor force, $\mathbf{F}_i^m(t)$, representing self-propulsion in a randomly chosen direction that remains constant during a running time τ. After every τ simulation time steps, particle i undergoes an instantaneous tumbling event, during which the

motor force is reoriented into a new random direction. The particle then runs in this new direction during the next time period τ before tumbling again. The running speed v is held constant. For an isolated particle in the absence of any barriers, the motor force produces a motion that is ballistic at short times and diffusive at very long times (29). If the particle does not collide with any other objects, then during a single running time it translates by one run length l_b, which is a distance of $l_b = |\mathbf{F}_i^{\mathrm{m}}|\tau/\eta$. The stochastic thermal force $\mathbf{F}_i^{\mathrm{T}}$ has the properties $\langle\mathbf{F}_i^{\mathrm{T}}(t)\rangle = 0$ and $\langle\mathbf{F}_i^{\mathrm{T}}(t)\mathbf{F}_j^{\mathrm{T}}(t')\rangle = 2\eta k_B T\,\delta_{ij}\delta(t - t')$. If $\mathbf{F}_i^{\mathrm{m}}(t) = 0$ so that the particles experience only thermal fluctuations but no motor force, then no rectification occurs. $\mathbf{F}_i^{\mathrm{S}}$ represents particle–particle interactions, whereas $\mathbf{F}_i^{\mathrm{B}}$ is the particle–barrier interaction term. The barriers and confining walls are modeled as exerting a short-range steric repulsion on particle i, and a particle interacting with a barrier or wall runs along the wall at a speed determined by the component of $\mathbf{F}_i^{\mathrm{m}}$ that is parallel to the wall until the particle reaches the end of the wall or undergoes a tumbling event that rotates its running direction away from the wall.

A simulated system in which particle–particle interactions and thermal fluctuations are both neglected, so that the particles experience only a motor force propulsion and interactions with the barriers and walls, is illustrated in **Figure 3a,b**. The sample is of size $L = 99a_0$ on a side, where a_0 is the unit of distance in the simulation, and contains 12 funnel barriers that each have a tip angle of 60° and an arm length of $l_f = 5a_0$. The running length is $l_b = 40a_0$, so a particle can move much farther than the length of a funnel arm during a single run time. The particle density is initially uniform, as shown in **Figure 3a**, but after a time 100τ, **Figure 3b** shows that the particle density has increased in the upper chamber. The ratio of the particle density $\rho^{(1)}$ in the upper chamber and $\rho^{(2)}$ in the lower chamber to the initial particle density ρ_b is plotted as a function of simulation time steps in **Figure 3c**. In a system with $l_b = 180$, the density in the upper chamber increases over time with a simultaneous decrease in the lower chamber density until the sample reaches a steady state. When the running length is very short, $l_b = 0.01$, the density in both chambers remains nearly constant at a value equal to the initial particle density. When l_b is very small, the particle motion is Brownian-like, so no rectification can occur. The steady-state ratio $r = \rho^{(1)}/\rho^{(2)}$ is plotted as a function of l_b in **Figure 4**. For small l_b, $r = 1$, whereas for large l_b, r reaches a value of nearly $r = 5.0$. The inset of **Figure 4** illustrates the ratchet mechanism. The left inset shows that under the wall-following rule of motion, when l_b is sufficiently large, a particle approaching the funnel barrier from the top chamber becomes trapped at the funnel tip until a tumbling event allows it to escape back into the top chamber, whereas a particle approaching the funnel barrier from below is shunted along the barrier wall into the top chamber. In the right inset, a particle with a very short run time spends very little time interacting with the wall, similar to a purely Brownian particle, and is unable to sample the barrier asymmetry over a timescale long enough to bias its motion toward the upper chamber. The two ingredients that are required to produce a ratchet effect are the running of particles along the walls and the breaking of detailed balance by the motor force. In the same simulation study, the rectification effect is reduced when a finite temperature is added because this increases the chance that a particle will prematurely move away from a wall. The ratchet effect is also reduced by the inclusion of steric particle–particle interactions because particle collisions effectively reduce the running length, whereas a buildup of particles in the funnel tip reduces the ability of the funnels to trap particles approaching from the upper chamber.

Figure 5a shows a snapshot from a simulation of run-and-tumble particles with steric particle–particle interactions moving between two chambers separated by funnel barriers. When the run length is sufficiently large (37), the inclusion of steric interactions produces two additional features: a buildup of particles along the walls, and trapping of particles in the funnel tips. Both of these effects were observed in the experiments of Reference 7. One question is whether the accumulation
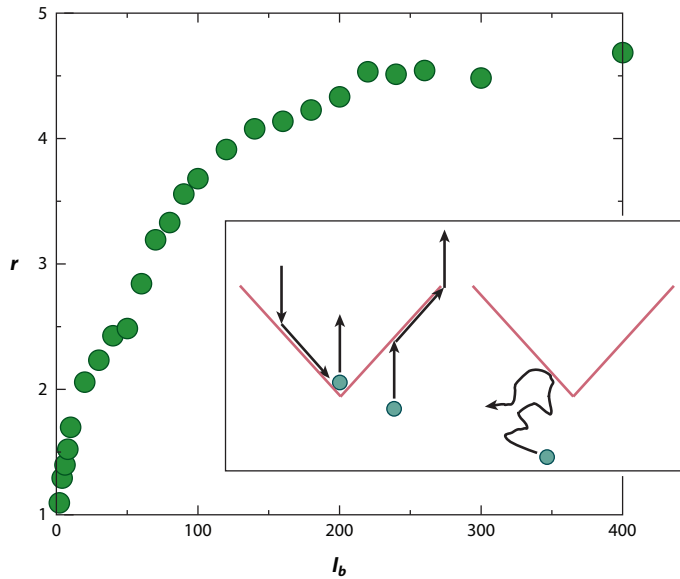
Figure 4

The ratio $r = \rho^{(1)}/\rho^{(2)}$ of the particle density in the upper chamber to that in the lower chamber for the system in **Figure 3** at steady state versus run length l_b, showing that for small run lengths $r = 1.0$ and no rectification is indicated, whereas for large l_b the ratio r reaches a value of nearly $r = 5.0$. (*Inset*) Schematic illustration of the rectification mechanism. On the left, an individual particle approaching the funnel barrier from above becomes trapped at the funnel tip, whereas a particle approaching from below is shunted by the funnel wall into the upper chamber. On the right, a Brownian particle spends very little time in contact with the funnel walls. Adapted from Reference 36 with permission, ©2008 by the American Physical Society.

of particles along the walls in the experiments is produced by hydrodynamic effects or whether it arises purely out of the self-propulsion of the bacteria. Using numerical and analytical methods, Tailleur & Cates (38) investigated run-and-tumble particles confined by a spherical trap and found that the dynamics alone produce particle accumulation on the walls. Other studies of confined active matter in which the motor force rotates diffusively also show a buildup of particle density along the walls, indicating that this effect is enhanced near corners (39, 40). The tendency of active matter particles to accumulate in corners is one of the reasons the funnel barriers can produce a ratchet effect, as the increased trapping occurs on only one side of the funnels due to their curvature. The work in Reference 41 also shows how the nature of the particle–wall interactions leads to rectification. Rectification by the funnel geometry is robust against changes in the running length distribution, as is observable by comparing these results with that of Wan et al. (36), who used only a single running length in each simulation, and of Tailleur & Cates (38), who considered a Poisson distribution of running lengths. Changes in the nature of the particle–wall interactions, however, can destroy the rectification. Four possible interaction rules are shown schematically in **Figure 5b–e**. Under Rule I, the motor force alignment is unchanged by contact with the wall, and the particle moves according to the component of the motor force vector that is parallel to the wall. In Rule II, the motor force is realigned to be parallel with the wall upon contact. For Rule III, the particle is reflected by the wall, whereas in Rule IV, the particle collides elastically with the wall. In Reference 38, when the motor force realigning Rule II is employed, efficient rectification of the particles occurs; however, if the elastic collisions of Rule IV are substituted, the rectification is lost, as shown in **Figure 6c**. An examination of the four wall rules in Reference 37
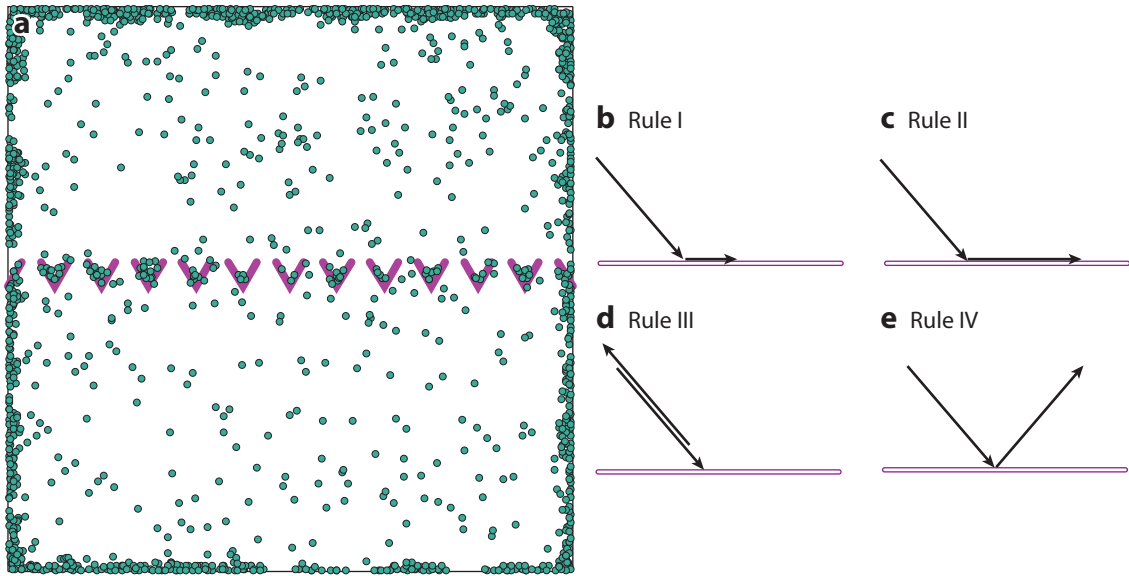
Figure 5

(*a*) Simulation image of the buildup of sterically interacting run-and-tumble particles along the walls and in the funnel-barrier tips for a system with a run length of $l_b = 120$. (*b–e*) Different possible particle–wall interaction rules. (*b*) Rule I: The particle maintains its original running direction and moves along the wall with the component of its velocity that is parallel to the wall. (*c*) Rule II: The particle realigns its running direction to be parallel with the wall. (*d*) Rule III: The particle reflects from the wall. (*e*) Rule IV: The particle undergoes an elastic collision with the wall. Ratchet effects occur for Rules I and II, with the strongest ratcheting for Rule II, but Rules III and IV produce no ratcheting. Adapted from Reference 37 with permission.

shows that the running of the particle along the wall, as in Rules I and II, is essential for producing a ratchet effect. When the particle does not remain in contact with the wall, as in Rules III and IV, the rectification is lost.

Follow-up experiments by Galajda et al. (42) using self-propelled, large-scale swimming bathtub toys produced a rectification effect similar to that observed for the bacteria, whereas experiments by Hulme et al. (43) demonstrate how the ratchet effect can be used to fractionate motile *E. coli* using arrays of asymmetric chambers of the type illustrated in **Figure 7a**. The arrows in **Figure 7b(i–v)** show how bacteria moving in the positive *x* direction are guided through the chamber array, whereas in **Figure 7b(vi–x)** bacteria moving in the negative *x* direction are blocked by the chamber geometry. Variations on similar channel geometries have been shown to produce guided motion of bacteria (44). Kim et al. use similar microfabricated ratchet channels with asymmetry to concentrate *E. coli* at particular locations (45).

Numerous other shapes can produce rectification of bacteria, such as the multiple rows of U-shaped funnel barriers illustrated in **Figure 8a** that produce rectification of particles with a motor force that rotates diffusively (46). In **Figure 8b**, a plot of the rectification ratio A_r, given by the ratio of the density in the right chamber to that in the left chamber, versus the motor force F_A for one, two, and three rows of barriers shows that A_r increases linearly with F_A and that there is a strong enhancement of the ratchet effect with the addition of more layers of funnels. In the same study, an examination of barriers made from open and closed triangles, U shapes, and half boxes indicates that barriers with an open shape always produce a larger rectification than barriers with closed shapes due to the trapping of particles within the tips of the open barriers.
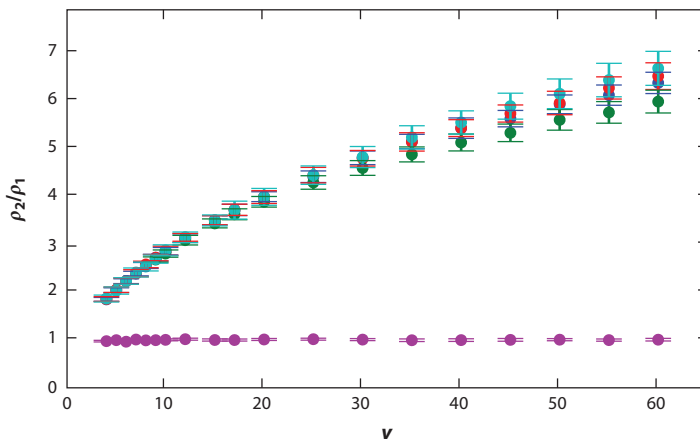
Theoretical and numerical studies show that rectification effects are a general phenomenon that occurs for self-driven particles in the presence of asymmetric piecewise periodic potentials (47, 48). In other numerical studies, the directed transport that occurs for self-propelled particles interacting with arrays of nonsymmetric convex obstacles without cavities was shown to result from the tendency of particles to attach to solid surfaces (49).

2.1. Sorting in Funnel Arrays

In numerical studies of the motion of active particles with a diffusively rotating motor force through funnel arrays, I. Berdakin et al. examined the effect of changing the swimming properties by varying the distribution of run lengths, the magnitude of the rotational diffusion, and the preservation of run orientation memory after a tumbling event (41). They observed that there are optimal swimming properties that maximize the rectification as a function of the geometry of the funnels. An illustration of the simulated funnel geometry appears in **Figure 9a** with colored dots indicating the positions of three different *E. coli* mutants modeled on the basis of characterizations performed by Berg & Brown (50). Species s1 represent CHeC497 with a mean run duration of 6.3 s and a speed of 20 µm/s; species s3 represent the wild-type AW405 with a mean run duration of 0.86 s and a speed of 14.2 µm/s; and species s4 represent Un602, which is the slowest species with a mean run duration of 0.42 s and a speed of 14.2 µm/s. The particles are initially placed along the leftmost wall, and after 12 min species s1, which have the longest run time and the highest speed, have moved the farthest to the right, followed by species s3, which move less far to the right, and finally by species s4, which show the least motion to the right. **Figure 9b** shows the number of bacteria as a function of time in the leftmost chamber (*decreasing curves*) and rightmost chamber (*increasing curves*), indicating that the different species become spatially separated over time. In follow-up studies, the same group observed that the use of multiple arrays of funnels enables the sorting of species that have only a small variation in a single swimming parameter (51).

a Forward direction

20 μm

b Cells entering from the left   Cells entering from the right

i · ii · iii · iv · v · vi · vii · viii · iv · x

50 μm
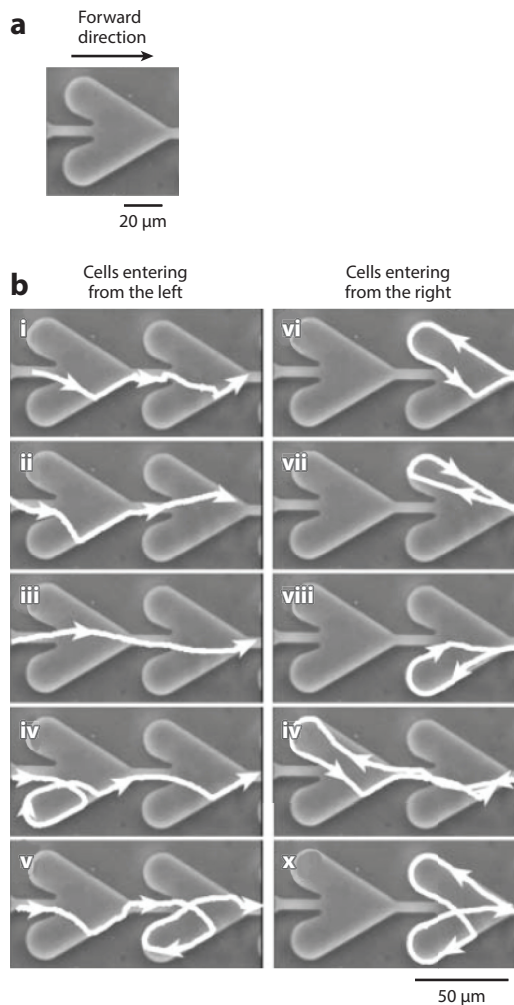
Figure 7

The motion of bacteria through an array of asymmetric chambers. (*a*) The geometry of a single chamber, indicating the easy flow direction. (*b*) Experimentally obtained trajectories of bacteria. Panels *i* through *v* show that bacteria can easily pass through the chambers for motion in the forward direction, whereas panels *vi* through *x* show that motion in the reverse direction is blocked owing to the chamber shape. Using this geometry it is possible to fractionate swimming bacteria that have different sizes or mobilities. Reproduced from Reference 43 with permission of The Royal Society of Chemistry. **http://dx.doi.org/10.1039/b809892a**.

2.2. Eukaryotic Cells and Swimming Animals in Funnel Arrays

The motion of biological cells through funnel geometries has been explored in several experiments. Kantsler et al. (52) considered swimming *Chlamydomonas* in both simulations and experiments using four chambers separated by funnel barriers; they measured the rectification ratio $R = \langle N_4 \rangle / \langle N_1 \rangle$, where $\langle N_4 \rangle$ is the steady-state number of cells in chamber 4 and $\langle N_1 \rangle$ is the steady-state number of cells in chamber 1. For funnels with a tip angle of 35°, $R = 4.0$, indicating strong rectification. In Reference 53, experiments on human sperm cells in quasi-2D microchambers containing funnel
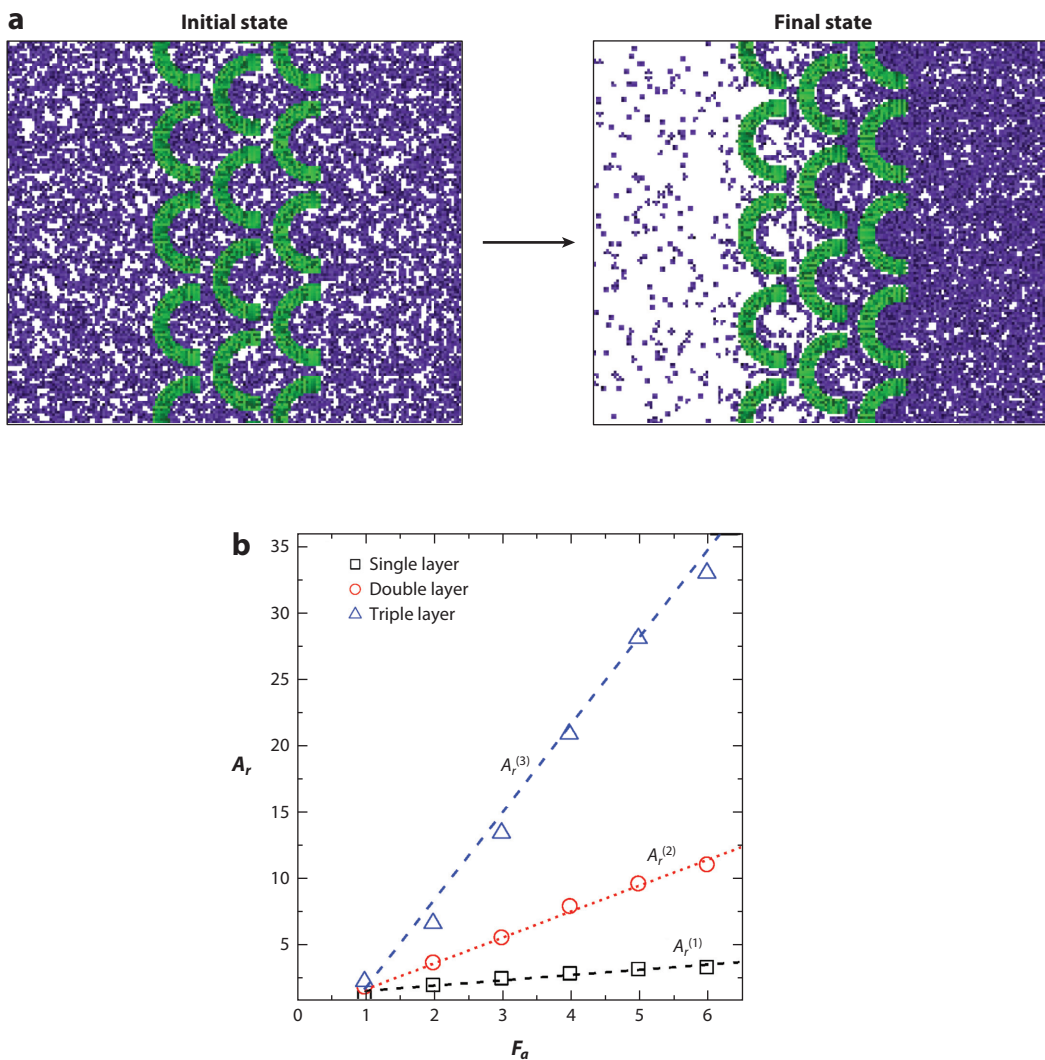
Figure 8

(*a*) Snapshots of the rectification effect in a simulation of particles with a motor force that rotates diffusively in two chambers separated by a triple layer of curved funnel barriers. The initial state with a uniform particle density is shown on the left, whereas the final state with the particles rectified in the easy flow direction into the right chamber is shown on the right. (*b*) The rectification ratio A_r—which is equal to the ratio of the density in the right chamber to the density in the left chamber, versus motor force F_a—for samples containing one (*squares*), two (*circles*), and three (*triangles*) layers of funnel barriers. Reproduced from Reference 46 with permission of The Royal Society of Chemistry. **http://dx.doi.org/10.1039/c5nr04124d**.

barriers showed that rectification occurs when the cells become trapped in the funnel tips. The same study showed that because the sperm are attracted to the boundaries, the ratchet effect can be optimized by using U-shaped barriers. Experiments with *Caenorhabditis elegans* moving through funnel barriers showed that the wild type, which moves along walls that it contacts, can be rectified by the barriers (54). In contrast, mutant strains that lack touch sensory neurons in
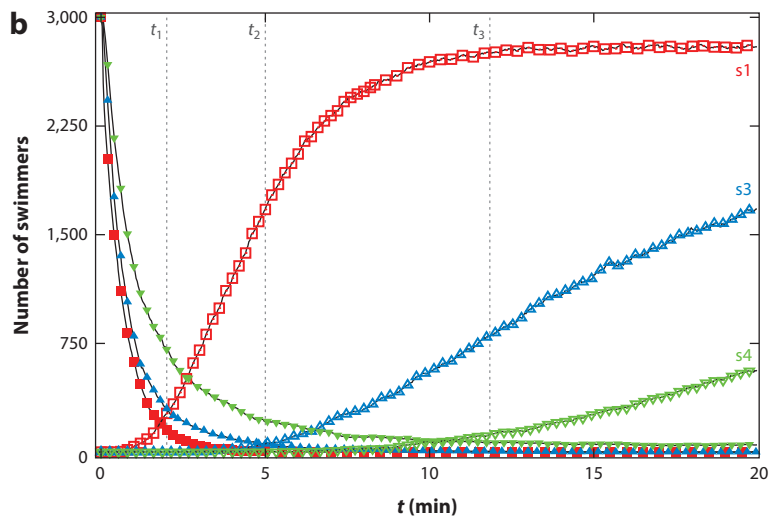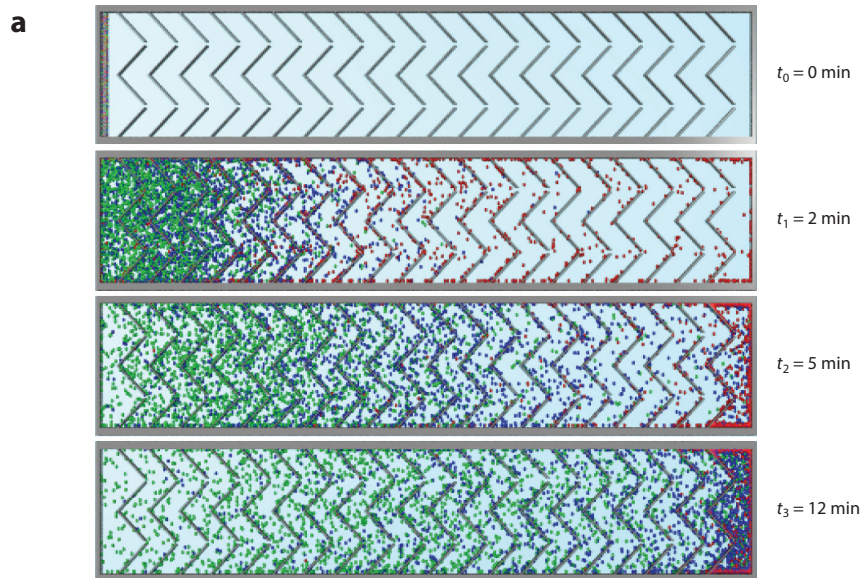
Figure 9

(*a*) Snapshots of simulated bacteria positions at different times for a mixture of three *Escherichia coli* mutants moving through a series of funnel barriers: red dots, CheC497 or s1 (fastest); blue dots, AW405 or s3; green dots, Ucn602 or s4 (slowest). The bacteria begin along the leftmost wall at time $t = 0$. (*b*) The number of bacteria versus time in the leftmost chamber (*solid symbols*) and the rightmost chamber (*open symbols*), showing that the different bacteria species can be fractionated using multiple funnel arrays. Reproduced from Reference 41 with permission, ©2013 by the American Physical Society.

their body reverse motion upon contacting a wall instead of following the wall, and these mutants are not rectified by the barriers.

2.3. Other Active Ratchet Geometries

A variety of other ratchet geometries for active particles have been studied, including 2D corrugated asymmetric substrates (55) and 2D geometries where entropic effects are important (56). Other works focus on the effect of changing the active particle shape to swimming ellipses (57) or on including an additional external drift force to the active particles to produce an active drift ratchet (58). Kulic et al. proposed that ratchet effects can occur in a variety of plants in which the asymmetry of the roots, seeds, or leaves is important for transport in the natural world where fluctuations may be present (59). Finally, in the case of symmetric substrates, periodically modulating the velocity of the active particles and then phase-shifting this velocity with respect to the substrate periodicity breaks enough symmetries to permit a ratchet effect to occur (60).

2.4. Future Directions

In ratchets produced using funnel barriers, it would be interesting to examine additional modes of motion of the active particles such as particles that avoid walls, particles that reverse their motion if the density is too high, or particles that change swimming strategies as a function of local density or of time. Many of the active matter ratchet studies performed so far employ infinitely repulsive barriers or walls; however, many previous studies of nonactive matter ratchet effects produced by external driving were performed for substrates containing pinning sites with a finite strength, so that a particle experiencing a sufficiently large driving force can pass through the pinning potential or barrier. It would be interesting to examine active matter particles moving through asymmetric finite-strength pinning arrays rather than obstacle arrays. Pinning arrays for colloidal particles can be readily created experimentally using optical means, so it should be possible to create optically generated pinning arrays for active colloidal particles or swimming bacteria. Additionally, optical traps introduce the possibility of creating flashing substrates, which could significantly enhance active matter ratchet effects. It was recently proposed that by using a light intensity pattern with a funnel or chevron shape to manipulate a dense assembly of sterically interacting active particles that are attracted by light, the patterned regions would become filled with trapped active particles that would then serve as an asymmetric substrate that can produce ratcheting motion of the remaining untrapped active particles (61). There has also been work examining how asymmetry in the curvature of the walls can produce different pressures on each side of the wall, producing a ratchet effect (62). This suggests that curvature is another route to explore in producing different types of active ratchet devices. Other possible systems to explore include crawling insects or animals. Studies that reveal boundary-following behaviors in animals (63) suggest that asymmetry in the boundaries could be used to produce ratchet effects. Another avenue of study is the introduction of feedback effects to a ratchet system, which could be achieved through optical methods. Recent studies of active matter using feedback controls have produced a variety of behavior for very simple feedback rules (64, 65).

3. COLLECTIVE ACTIVE MATTER EFFECTS

3.1. Active Ratchet Reversals

In rocking and flashing ratchet systems, a rich variety of collective effects including ratchet reversals arise when particle–particle interactions are included (2–5). For run-and-tumble active particles

moving through funnel barriers, Wan et al. observed that the addition of steric particle–particle interactions produced only a monotonic reduction in the rectification effect (36). Drocco et al. (66) placed particles obeying a Vicsek model, modified to include particle–barrier interactions and steric particle–particle interactions with an exclusion radius r_e, in a funnel-barrier geometry. For small r_e, the particles ratchet in the easy flow direction, and the magnitude of the ratchet effect depends on the noise term η in the Vicsek model. For small η the system forms flocks, whereas for large η the system is in a liquid-like state. In the funnel-barrier system, the ratchet effect is strongly reduced or completely lost for large η, whereas for small η in which flocking occurs, a pronounced ratchet effect appears with density ratios in the two chambers approaching $r = 5.0$. **Figure 10b,c** highlights the enhancement of the ratchet effect due to the collective rectification of groups of active particles. In **Figure 10b**, a flock approaches the funnel barriers from below. The flock becomes compressed and moves through the barrier array as a unit, as illustrated in **Figure 10c**. A reversal of the ratchet effect, in which the particles collect in the bottom chamber in the hard flow direction of the funnel barriers, can occur when flocks are present. **Figure 10a** shows a plot of the particle density in the top chamber ρ_{top} versus the particle exclusion radius r_e for a system in which $\eta = 1.5$, the flocking radius is 1.0, the starting uniform density is $\rho = 0.4$, and the closest spacing between adjacent funnel barriers is $l_0 = 0.6$. For $0.0 < r_e < 0.1$, rectification occurs in the easy flow direction of the funnel barriers as illustrated in **Figure 10b,c**, but there is a reversal of the rectification in the hard flow direction for $0.1 \leq r_e < 0.3$. For $r_e \geq 0.3$, the diameter of the particles is larger than the closest spacing between funnels, $r_e \geq l_0$, so it is no longer possible for particles to pass between the upper and lower chambers, and the rectification effect is lost. The ratchet reversal is produced by a jamming effect that occurs during the compression of a flock of particles as it approaches the opening between adjacent funnel barriers from below. The compression causes the particles at the leading edge of the flock to form a rigid close-packed structure that is wider than the interfunnel spacing l_0, making it impossible for the flock to cross the line of funnel barriers. In contrast, when a flock approaches the funnel barriers from above, the barriers cleave the flock into smaller clusters, and during this process one or two particles can escape from the flock and pass between the funnel barriers to enter the lower chamber. This reversed motion process always occurs but cannot compete with the forward motion of flocks of particles moving into the top chamber for small r_e. When the forward motion is inhibited by jamming at larger r_e, the reversed motion dominates and a reversed ratchet effect appears. The reverse ratchet effect operates much more slowly than the forward ratchet effect, so a much longer time is required for the system to reach a steady state in the reverse ratchet regime than in the forward ratchet regime. If two species of particles with different exclusion radii of $r_e = 0.055$ (small) and $r_e = 0.22$ (large) are placed in the container, flocks of the different species ratchet in opposite directions and can be spatially separated, as shown in **Figure 11**.

Ratchet reversals have also been observed for eukaryotic cells moving on asymmetric substrates. Mahmud et al. (67) examined cell motility on micropatterned ratchet surfaces. They considered cancerous B16F1 cells (which are a mouse epithelial-like melanoma cell), noncancerous Rat2 fibroblast cells, and cancerous MDA-MB-231 human mammary gland cells. For the B16F1 and Rat2 cells, directed motion occurs along the easy flow direction of the funnel array. The addition of a protruding spike shape to the funnel-shaped chambers does not affect the Rat2 cells, which still ratchet in the easy direction, but causes the B16F1 and MDA-MB-231 cells to perform a reversed ratchet motion in the hard flow direction. The differences in the direction of the ratchet motion for the different cells were attributed to the different crawling mechanisms of the cells. Rat2 cells use long protrusions that can grab the funnel edges or the ends of the spike shapes, whereas the other cells prefer to spread out in the open spaces as they move. Mahmud et al. also found that it is possible to use arrays of the spike-shaped funnels to separate a mixture of different
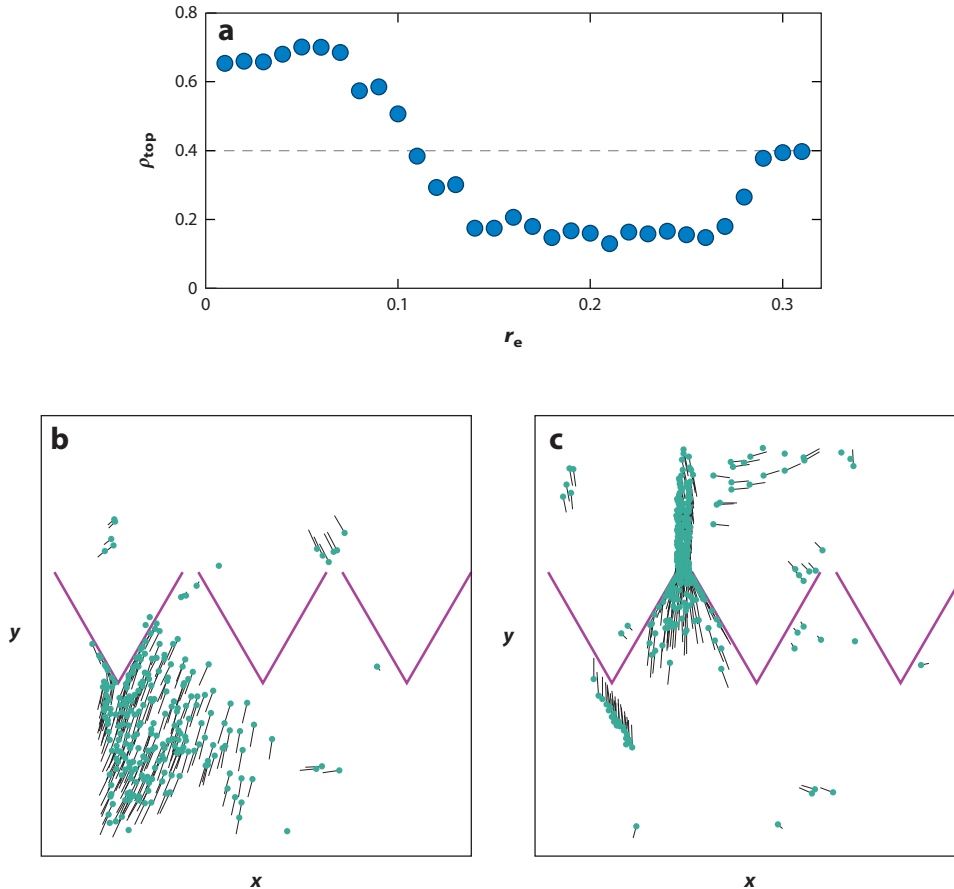
Figure 10

Simulations of sterically interacting flocking particles in a funnel-barrier array. (*a*) Steady-state density ρ_{top} of particles in the upper chamber versus the particle exclusion radius r_e. The dashed line indicates the uniform starting density with $\rho_{top} = \rho_{bottom} = 0.4$. The ratchet effect in the easy flow direction is maximized for small r_e. A reversal in the ratchet direction occurs for $0.1 < r_e < 0.3$, and the ratchet effect is lost for $r_e > 0.3$ when the particles become too large to fit between adjacent funnels. (*b,c*) Images of a small portion of the sample illustrating the forward rectification mechanism. (*b*) A flock approaches the funnel barriers from below. (*c*) The flock elongates and passes through the barrier array as a unit. Adapted from Reference 66 with permission, ©2012 by the American Physical Society.

cells over time, and they propose the creation of a bidirectional ratchet, opening the possibility of creating cell traps and ratchets to achieve various types of medical treatments. Other studies have shown that unidirectional cell motion can be achieved using asymmetric nanotopography (68).

3.2. Active and Passive Ratchet Mixtures

Self-propelled Janus colloids, whose direction of motion slowly diffuses rotationally, represent another type of experimental artificial active matter system. Ghosh et al. (69) performed simulations of active Janus particles in an asymmetric channel and observed that rectification occurs in the easy flow direction of the channel and that the magnitude of the ratchet effect increases
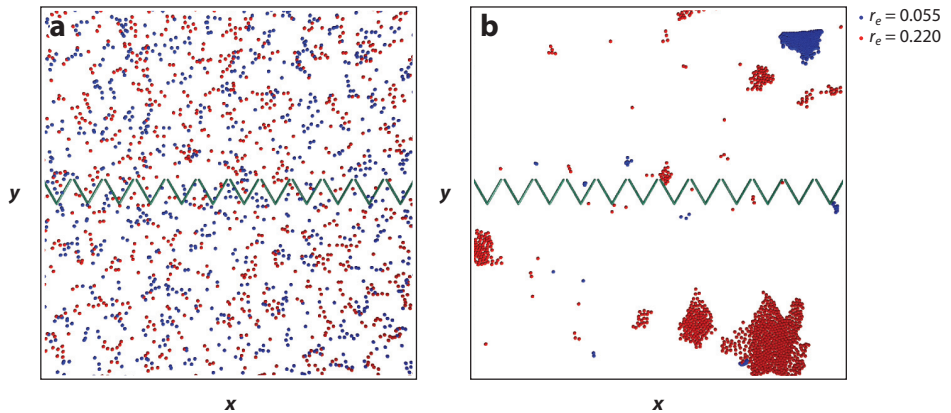
Figure 11

Images from simulations of sterically interacting flocking particles with two different exclusion radii, $r_e = 0.055$ (small particles, *blue*) and $r_e = 0.22$ (large particles, *red*). (*a*) The initial configuration with uniform density in both top and bottom chambers, which are separated by a line of funnel barriers. (*b*) A representative steady-state configuration at a later time. The larger red particles undergo reversed rectification and collect in the bottom chamber, whereas the smaller blue particles undergo forward rectification and collect in the top chamber.

with increasing correlation time of the particle running direction, eventually saturating for large correlation times. They also considered a mixture of N_m active particles and N_p nonactive particles in the same geometry, with the particle–particle interactions modeled as a repulsive harmonic force, and found that the active particles can induce a net rectification of the nonactive particles. A particularly interesting effect is that the rectification transport flux for the nonactive particles is nonmonotonic as a function of particle density. For one choice of parameters, the maximum nonactive particle ratchet transport flux occurs for a ratio of $N_p/N_m = 12$, indicating that even a very small fraction of active particles can efficiently rectify the passive particles. In the dense limit of $\phi = 1.0$ close to the jamming regime, Ghosh et al. find a small reversal of the ratchet effect.

In experiments with passive colloids immersed in a bath of swimming bacteria, Koumakis et al. showed that introducing an asymmetric substrate that causes the bacteria to undergo rectification also produces transport of the passive colloids into or out of enclosed regions (70). **Figure 12*a*** shows the time evolution of the number of passive colloids in each chamber of a sample containing three layers of ratchets for a geometry that concentrates the colloids in the central chamber, whereas **Figure 12*b*** shows the same quantity for a geometry that ejects the colloids from the box. Koumakis et al. also found that curved ratchet geometries were not as efficient as flat boundaries in their device because the colloids would follow curved trajectories over the curved surfaces. These results show how collective effects in active ratchets could be used to achieve a variety of active pumping techniques. It may also be possible that biological systems such as cells already take advantage of such collective ratchet effects.

3.3. Future Directions

The field of collective effects in active matter systems is wide open. Because a wide variety of flocking models exist, it would be interesting to determine what types of ratchet effects occur for different flocking rules. This would also be an interesting question to examine in experiments on schools of fish or swarming insects, which could be placed in funnel-like channels, with a
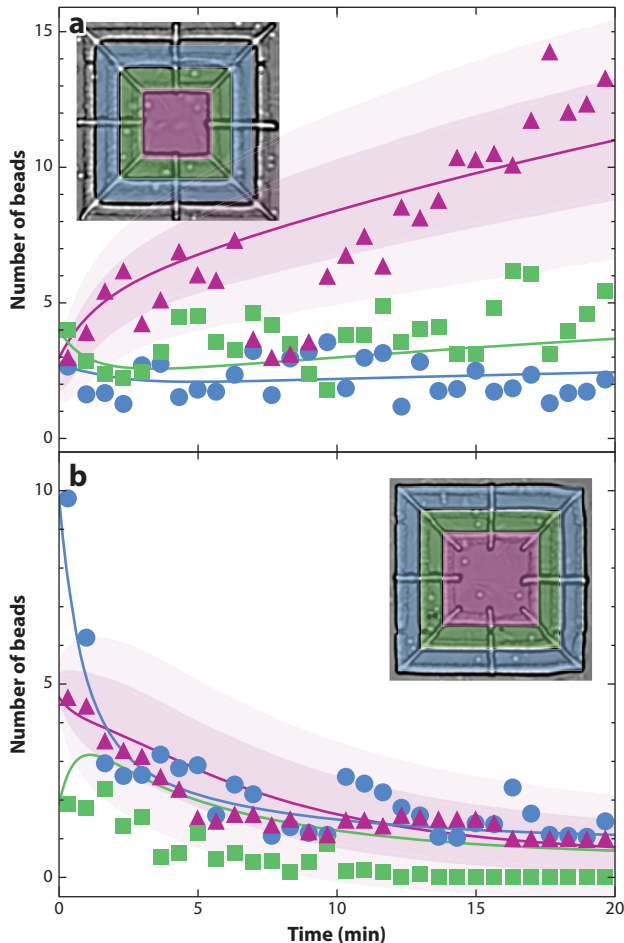
Figure 12

Experimental demonstration of the directed motion of passive colloids immersed in a bath of bacteria that interact with a ratchet geometry. The plots indicate the number of passive particles in each chamber or spatial region, color coded according to the inset. (*a*) A geometry that concentrates the passive particles at the center of the device. (*b*) A geometry that ejects the passive particles from the center of the device. Reproduced from Reference 70 with permission from MacMillan Publishers Ltd.: *Nature Communications*, ©2013.

comparison of ratchet behaviors between schooling and nonschooling systems. Similar experiments could be performed with herding animals. It would also be interesting to explore systems with competing effects, such as a ratchet geometry that biases the motion of the system in one direction combined with some other competing force that biases the motion of the system in the opposite direction. In such a case, it is possible that flocking or collective effects could be turned on or off to take advantage of or nullify the ratchet effect. There has already been some evidence for competing interactions that can overwhelm the ratchet effect, such as an experiment on bacteria in a funnel-barrier ratchet geometry, where the bacteria form Fisher wave swarms that move against the ratchet direction (71).

Self-driven colloids exhibit a phase separation transition into gas-like and clustered solid-like phases for high enough density or activity (31–34), so it would be interesting to examine how the

ratchet transport flux is affected by the onset of self-clustering. Introduction of a substrate can modify the density or activity at which the self-clustering begins to occur, as well as the mean distance that individual particles can move (72). Collective ratchet effects should also depend strongly on the type of interactions between the particles. In the systems studied so far, short-range steric repulsion has been used for the particle–particle interactions; however, it is also possible to consider active particles with Lennard–Jones interactions, long-range repulsive interactions, competing long-range repulsion and short-range attraction, or many-body interactions.

Another class of system is active membranes or sheets that could mimic cells or collections of tightly bound organisms. Swimming deformable droplets are one example of an extended active object of this type (73), and if such droplets were placed on an asymmetric surface, ratchet effects could occur. In this case, varying the substrate periodicity to be larger or smaller than the size-scale of the active object could cause changes in the ratchet effect. There has already been a study demonstrating ratchet effects for active polymers in funnel-barrier arrays (74). Other motion rules could also be introduced to model objects that have mechanics similar to cells, such as protrusions that push or pull, for mimicking the experiments in Reference 67. There could also be ratchet effects for extended active objects that can expand or contract, such as a squirmer model or a system with inertial dynamics.

Collective ratchet effects can also be examined for groups of interacting rods coupled with molecular motors when an additional asymmetry is introduced, or active gel systems such as active nematics (75, 76) could be studied in the presence of an asymmetric substrate. Active nematics can also exhibit mobile defects (77, 78), so it may be possible to produce ratcheting motion of the defects.

4. RATCHETS IN CIRCLE SWIMMERS AND CHIRAL SYSTEMS

There are many examples of active biological and artificial systems that exhibit a chirality in their motion, such as biological circle swimmers (79–81) and artificial circle swimmers (82–84). In these cases, ratchet effects can occur even in the absence of a substrate asymmetry because the chirality of the swimming introduces an asymmetry to the system. One of the first examples of a ratchet effect produced by chirality was observed for circularly moving particles on a 2D periodic substrate (85). As the substrate-free particle orbits are varied from circular to more complex Lissajous patterns, a series of transitions occurs between localized closed trajectories with no net translation to open trajectories that permit the particles to translate in a particular direction, producing a ratchet effect. Additional simulations have shown that directed motion can be achieved for circularly moving particles on periodic substrates, where various types of translating trajectories appear (86), whereas in experiments with circularly moving colloids on 2D substrates, directed or ratchet motion can be produced (87). Nourhani et al. (88) considered a model of counterclockwise circle swimmers on a 2D periodic substrate for both deterministic and stochastic swimmers. In the deterministic regime they found that the particles can either form closed orbits or translate at fixed angles with respect to the substrate periodicity. In the stochastic regime, the ratchet effect extends over a wider range of parameters because the particles can hop between different rectifying orbits even if they become temporarily trapped in a closed or nonrectifying orbit.

It is also possible to obtain ratchet effects for circle swimmers moving over asymmetric substrates (89). **Figure 13a** shows a counterclockwise swimming particle moving with a motor force amplitude of $A = 0.57$ over an array of L-shaped barriers. The particle translates one substrate lattice constant in the positive y direction during every swimming cycle. For $A = 0.9$ in **Figure 13b**, the particle is confined to a closed nontranslating orbit. In **Figure 13c**, the translating orbit at $A = 1.5$ includes particle motion in both the positive x and positive y directions.
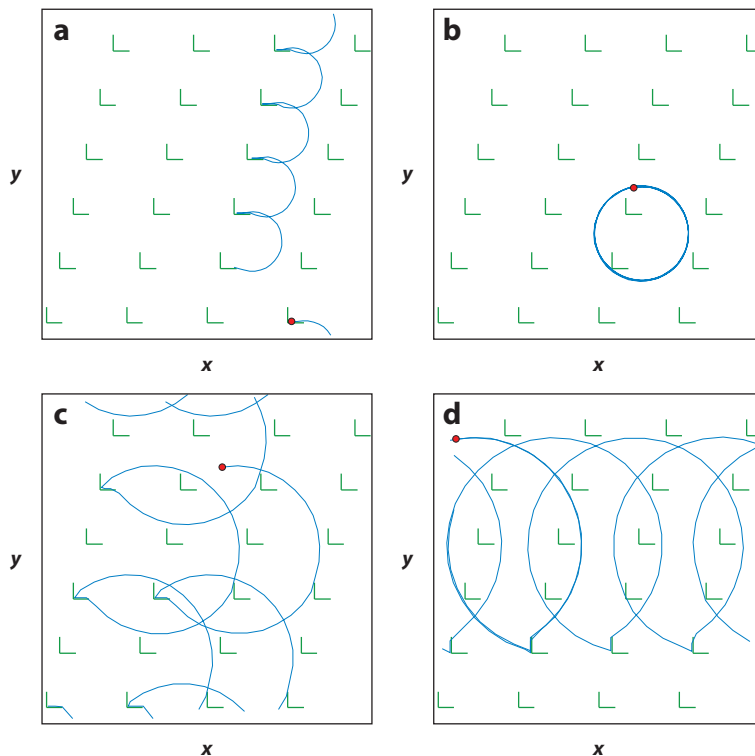
Figure 13

The particle orbits from a simulation of circle swimmers in an array of L-shaped barriers. (*a*) At a motor force of $A = 0.57$, translation occurs in the positive y direction. (*b*) For $A = 0.9$, a nonratcheting orbit appears. (*c*) At $A = 1.6$, the particle translates in the positive x and y directions. (*d*) At $A = 2.05$, the particle translates in the negative x direction. Adapted from Reference 89 with permission, ©2013 by the American Physical Society.

Figure 13*d* shows that at $A = 2.05$ the particle translates in the negative x direction. The average drift velocity of the particle in the y direction, $\langle V_y \rangle$, and in the x direction, $\langle V_x \rangle$, is plotted as a function of A in **Figure 14**. A series of quantized orbits occur in which the particle translates in a fixed direction over a finite interval of A. Due to the asymmetry of the L-shaped barriers, the locations of the translating or ratcheting regimes differ for clockwise and counterclockwise swimming particles; however, in general, swimmers with different chirality move in different directions, permitting a mixture of chiral swimmers to be separated by the barrier array. When thermal effects are included, the additional noise expands the range of values of A over which rectification occurs; however, the transport flux of the maximum ratchet effect is reduced compared to the nonthermal or deterministic limit.

Mijalkova & Volpe (90) considered the separation of different species of circle swimmers with different angular velocities by an asymmetric comb channel with a geometry that could be nanofabricated, as illustrated in **Figure 15*a***. The particles are initially placed in the leftmost chamber, and as time progresses, the particles moving at 2.2 rad/s undergo the largest amount of ratcheting motion along the channel, as shown by the histograms of particle density at different times in **Figure 15*b–e***. At the longest times of $t = 10,000$ s in **Figure 15*e*** the spatial separation of the different particle species is clearly visible.
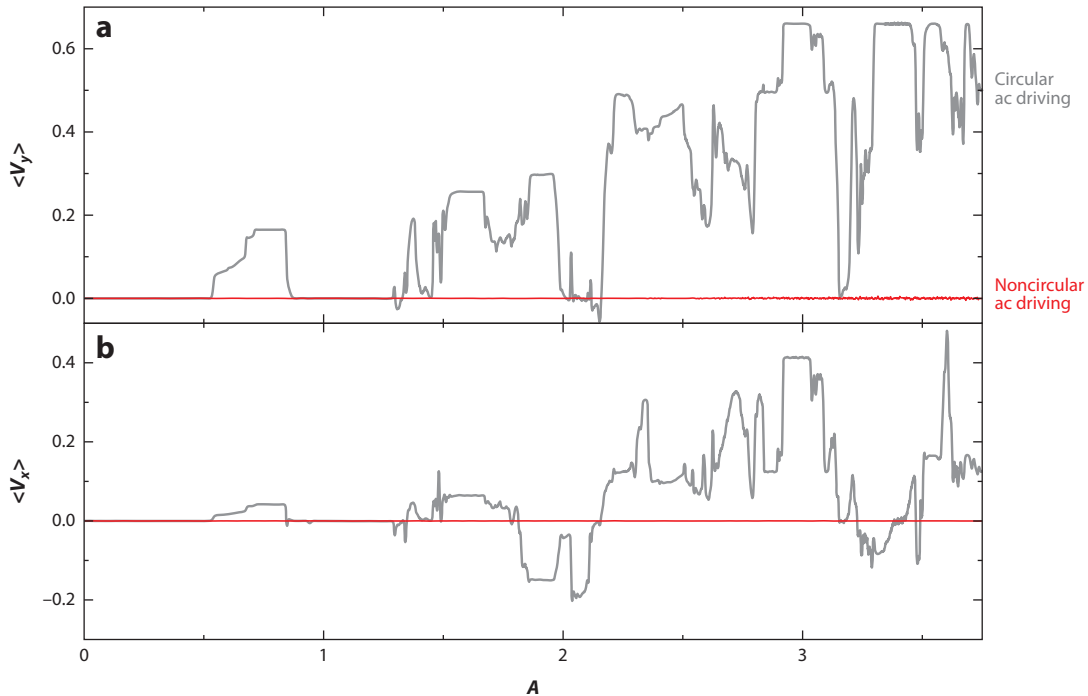
Figure 14

The net velocity of the circularly swimming particle from the system in **Figure 13** showing a series of ratchet orbits as a function of the motor force amplitude A. (*a*) $\langle V_y \rangle$ versus A. (*b*) $\langle V_x \rangle$ versus A. If the particle swimming direction is reversed from counterclockwise to clockwise, a different set of rectification phases occurs due to the asymmetry of the L-shaped barriers. Adapted with permission from Reference 89 with permission, ©2013 by the American Physical Society.

Ai et al. (91) considered chiral swimmers interacting with an array of half-circle barriers and found that particles with different chirality migrate to opposite sides of the sample due to interactions with the barriers. In a numerical study of chiral swimmers in a geometry containing M-shaped barriers on the bottom of the sample at $y = 0$ and periodic boundary conditions in the x direction, the chirality of the swimmers leads to a rectification effect and makes it possible to achieve the transport of a larger passive particle (92). The direction in which the active particles ratchet depends on the chirality of the swimming, so that counterclockwise and clockwise swimmers move in opposite directions. One of the surprising results of this work is that the direction in which the passive particle drifts can, for some parameters, be opposite to the direction in which the swimmers are moving, and this directional reversal depends strongly on the packing fraction of the system, which again indicates that collective effects can introduce new behaviors.

5. VARIANTS ON RATCHET-INDUCED TRANSPORT

Ratchet effects are generally studied in systems with fixed asymmetric substrates; however, if the substrate is mobile and can respond to the active particle, an active ratchet effect can occur that can be used to transport larger-scale asymmetric objects. Angelani et al. (93) examined a model of run-and-tumble bacteria interacting with large-scale passive rotary objects that have asymmetric sawtooth shapes. The bacteria accumulate in the corners of the "sawteeth" and generate a net torque that produces a persistent rotation of the object in one direction. Such active
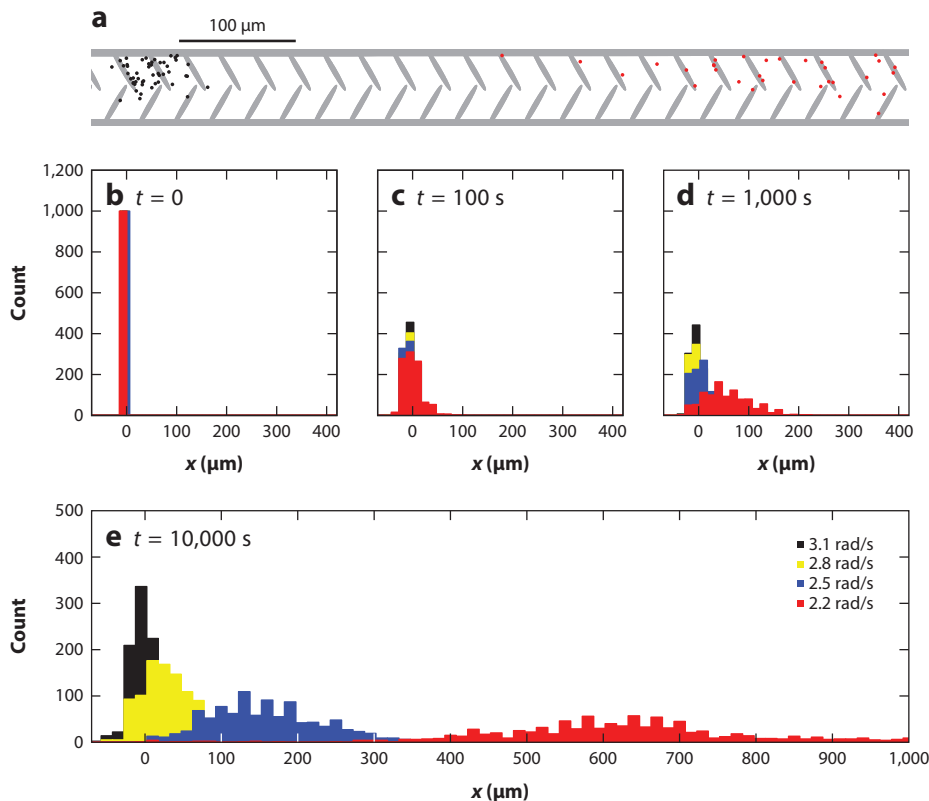
Figure 15

Simulations of the separation of circle swimmers with different angular velocities by an asymmetric comb channel with the geometry illustrated in panel *a*. The particles have angular velocities of 3.1 (*black*), 2.8 (*yellow*), 2.5 (*blue*), and 2.2 (*red*) rad/s. (*b–e*) Histograms of the particle positions for increasing times. The particles rotating at 2.2 rad/s exhibit the largest amount of rectification. Reproduced from Reference 90 with permission of The Royal Society of Chemistry.

matter–induced gear rotation was subsequently confirmed in several experiments with swimming bacteria (94–96) as well as for gears interacting with small robots (97). Additionally, if an asymmetric object is placed in a bath of active particles, it is possible to generate enhanced transport of the object. **Figure 16*a,b*** shows images of asymmetric objects placed in a bath of rod-like bacteria to create microshuttles (98). The bacteria, which swim in the direction of their white tips, accumulate in the corners of each shuttle object and produce a net force f that causes the shuttle to translate. **Figure 16*c*** shows that the probability distribution of f shifts its weight to higher values of f as the shuttle length is increased, producing a larger biasing propulsion force.

Experiments on asymmetric wedges in bacterial baths reveal enhanced transport of these objects (99), and other studies have examined how the shape of the asymmetric passive object affects the transport of the object (100). Because active particles accumulate in corners or concave regions of a funnel shape, it is possible to use static (101) or moving wedges (102) to capture active particles. Many variations using active matter to transport passive objects are possible. It would also be interesting to study systems in which the passive objects could change shape in response to the activity.
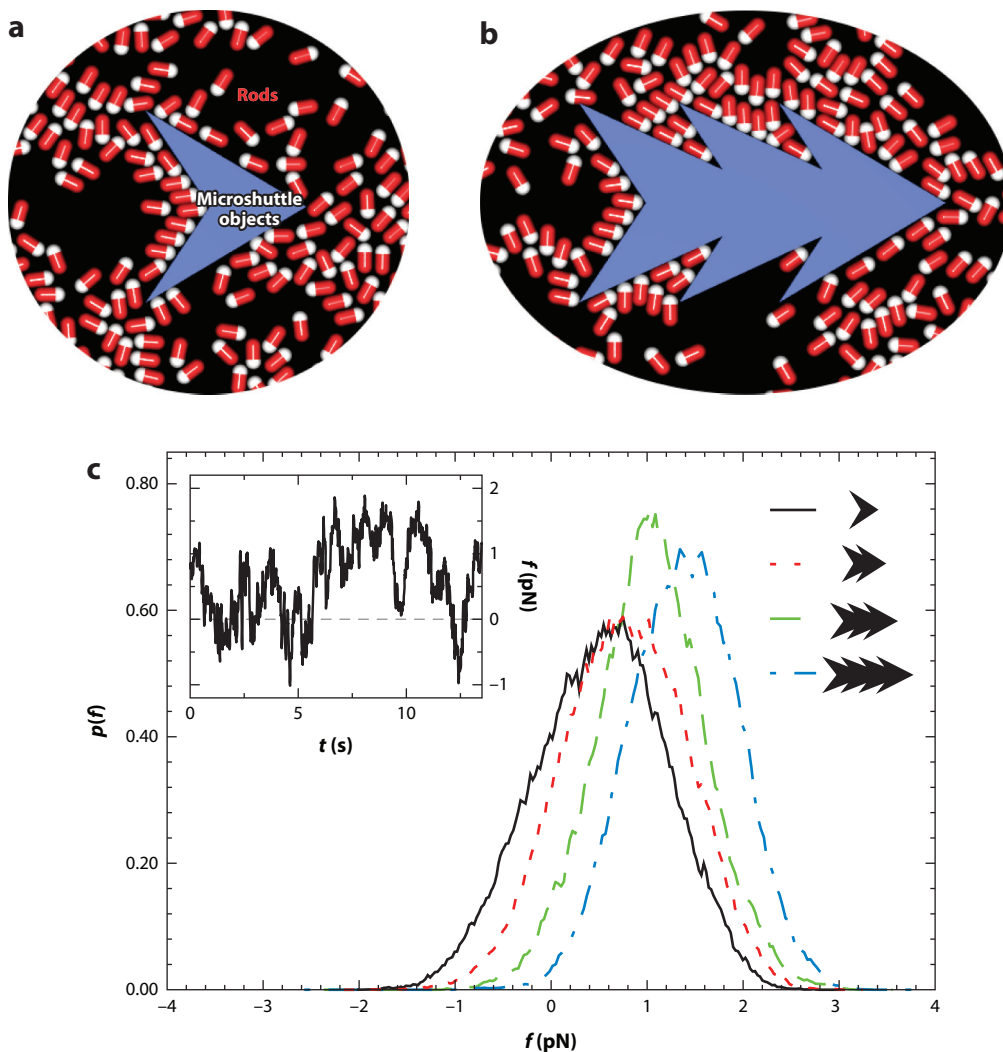
Figure 16

(*a,b*) Snapshots from simulations of asymmetric microshuttle objects (*blue*) interacting with self-propelled rods (*red with white*). The rods move in the direction of their white tips. (*a*) A shuttle composed of a single wedge shape moves when the active particles accumulate along the left side of the wedge. (*b*) Particles accumulate at each corner of a shuttle composed of three wedge shapes. (*c*) The probability distribution $p(f)$ of the time-averaged force f in picoNewtons (pN) exerted on the shuttle by the active particles for shuttles made from 1 (*black*), 2 (*red*), 3 (*green*), or 4 (*blue*) wedges, showing an increase in the effective driving force as the number of wedges increases. Reproduced from Reference 98 with permission, ©IOP Publishing & Deutsche Physikalishe Gesellschaft. CC BY-NC-SA. **http://dx.doi.org/10.1088/1367-2630/12/11/113017**.

6. CONCLUSION

We have highlighted the recent results for a new class of ratchet system called active ratchets, which appear when the directed motion of self-propelled particles, which breaks detailed balance, is combined with an additional asymmetry in the system. Unlike rocking and flashing ratchets, active ratchets do not require the application of an external driving force to produce rectification. Active ratchet effects and variations on them will continue to be a growing field of research as the

ability to fabricate additional types of artificial swimmers, nanobots, and other self-driven systems continues to improve and the possibility of applying simple motion rules to the active objects that can permit them to perform usable work grows. Due to the general nature of the conditions under which active ratcheting can occur, it is likely that nature may already be exploiting active ratchet effects in various biological systems, so it would be interesting to examine motility processes in complex biological environments to understand whether active ratchet effects are present. Another area for future research is the collective effects that arise in assemblies of interacting active particles or in more complex objects such as cells. It has already been demonstrated that collective effects can produce a variety of novel ratcheting effects including ratchet reversals, which offers the possibility to utilize bidirectional ratchets for various medical technologies and other types of biological applications.

DISCLOSURE STATEMENT

ACKNOWLEDGMENTS

LITERATURE CITED

1. Reichhardt C, Reichhardt CJO. 2017. *Rep. Prog. Phys.* In press. arXiv:1602.03798
2. Reimann P. 2002. *Phys. Rep.* 361:57–265
3. Derényi I, Vicsek T. 1995. *Phys. Rev. Lett.* 75:374–77
4. de Souza Silva CC, Van de Vondel J, Morelle M, Moshchalkov VV. 2006. *Nature* 440:651–54
5. Lu Q, Reichhardt CJO, Reichhardt C. 2007. *Phys. Rev. B* 75:054502
6. Lee CS, Jankó B, Derényi I, Barabási AL. 1999. *Nature* 400:337–40
7. Galajda P, Keymer J, Chaikin P, Austin R. 2007. *J. Bacteriol.* 189:8704–7
8. Reichhardt C, Ray D, Reichhardt CJO. 2015. *Phys. Rev. B* 91:184502
9. Van Oudenaarden A, Boxer SG. 1999. *Science* 285:1046–48
10. Ertas D. 1998. *Phys. Rev. Lett.* 80:1548–51
11. Duke TAJ, Austin RH. 1998. *Phys. Rev. Lett.* 80:1552–55
12. Reichhardt CJO, Reichhardt C. 2005. *Physica C* 432:125–32
13. Dinis L, Perez de Lara D, Gonzalez EM, Anguita JV, Parrondo JMR, Vicent JL. 2009. *New J. Phys.* 11:073046
14. Reichhardt C, Reichhardt CJO. 2016. *Phys. Rev. B* 93:064508
15. Lindner B, Schimansky-Geier L, Reimann P, Hänggi P, Nagaoka M. 1999. *Phys. Rev. E* 59:1417–24
16. Reichhardt C, Ray D, Reichhardt CJO. 2015. *New J. Phys.* 17:073034
17. Rousselet J, Salome L, Ajdari A, Prost J. 1994. *Nature* 370:446–48
18. Farkas Z, Tegzes P, Vukics A, Vicsek T. 1999. *Phys. Rev. E* 60:7022–31
19. Wambaugh JF, Reichhardt C, Olson CJ. 2002. *Phys. Rev. E* 65:031308
20. Jones PH, Goonasekera M, Renzoni F. 2004. *Phys. Rev. Lett.* 93:073904
21. Salger T, Kling S, Hecking T, Geckeler C, Morales-Molina L, Weitz M. 2009. *Science* 326:1241–43
22. Linke H, Humphrey TE, Löfgren A, Sushkov AO, Newbury R, et al. 1999. *Science* 286:2314–17
23. Roeling EM, Germs WC, Smalbrugge B, Geluk EJ, de Vries T, et al. 2011. *Nat. Mater.* 10:51–55
24. Pérez-Junquera A, Marconi VI, Kolton AB, Álvarez-Prado LM, Souche Y, et al. 2008. *Phys. Rev. Lett.* 100:037203

25. Franken JH, Swagten HJM, Koopmans B. 2012. *Nat. Nanotechnol.* 7:499–503
26. Chat'e H, Ginelli F, Grégoire G, Peruani F, Raynaud F. 2008. *Eur. Phys. J. B* 64:451–56
27. Ramaswamy S. 2010. *Annu. Rev. Condens. Matter Phys.* 1:323–45
28. Marchetti MC, Joanny JF, Ramaswamy S, Liverpool TB, Prost J, et al. 2013. *Rev. Mod. Phys.* 85:1143–89
29. Bechinger C, Di Leonardo R, Löwen H, Reichhardt C, Volpe G, Volpe G. 2016. *Rev. Mod. Phys.* 88:045006
30. Cates ME, Marenduzzo D, Pagonabarraga I, Tailleur J. 2010. *PNAS* 107:11715–20
31. Fily Y, Marchetti MC. 2012. *Phys. Rev. Lett.* 108:235702
32. Redner GS, Hagan MF, Baskaran A. 2013. *Phys. Rev. Lett.* 110:055701
33. Palacci J, Sacanna S, Steinberg AP, Pine DJ, Chaikin PM. 2013. *Science* 339:936–40
34. Buttinoni I, Bialké J, Kümmel F, Löwen H, Bechinger C, Speck T. 2013. *Phys. Rev. Lett.* 110:238301
35. Reichhardt C, Reichhardt CJO. 2014. *Soft Matter* 10:7502–10
36. Wan MB, Reichhardt CJO, Nussinov Z, Reichhardt C. 2008. *Phys. Rev. Lett.* 101:018102
37. Reichhardt CJO, Drocco J, Mai T, Wan MB, Reichhardt C. 2011. *Proc. SPIE* 8097:80970A
38. Tailleur J, Cates ME. 2009. *Europhys. Lett.* 86:60002
39. Fily Y, Baskaran A, Hagan MF. 2014. *Soft Matter* 10:5609–17
40. Fily Y, Baskaran A, Hagan MF. 2015. *Phys. Rev. E* 91:012125
41. Berdakin I, Jeyaram Y, Moshchalkov VV, Venken L, Dierckx S, et al. 2013. *Phys. Rev. E* 87:052702
42. Galajda P, Keymer J, Dalland J, Park S, Kou S, Austin R. 2008. *J. Mod. Opt.* 55:3413–22
43. Hulme E, DiLuzio WR, Shevkoplyas SS, Turner L, Mayer M, et al. 2008. *Lab Chip* 8:1888–95
44. Kaehr B, Shear JB. 2009. *Lab Chip* 9:2632–37
45. Kim SY, Lee ES, Lee HJ, Lee SY, Lee SK, Kim T. 2010. *J. Micromech. Microeng.* 20:085007
46. Chen Y-F, Xiao S, Chen H-Y, Sheng Y-J, Tsao H-K. 2015. *Nanoscale* 7:16451–59
47. Angelani L, Costanzo A, Di Leonardo R. 2011. *Europhys. Lett.* 96:68002
48. Yariv E, Schnitzer O. 2014. *Phys. Rev. E* 90:032115
49. Potiguar FQ, Farias GA, Ferreira WP. 2014. *Phys. Rev. E* 90:012307
50. Berg HC, Brown DA. 1972. *Nature* 239:500–4
51. Berdakin I, Silhanek AV, Cortéz HNM, Marconi VI, Condat CA. 2013. *Cent. Eur. J. Phys.* 11:1653–61
52. Kantsler V, Dunkel J, Polin M, Goldstein RE. 2013. *PNAS* 110:1187–92
53. Guidobaldi A, Jeyaram Y, Berdakin I, Moshchalkov VV, Condat CA, et al. 2014. *Phys. Rev. E* 89:032720
54. Nam S-W, Qian C, Kim SH, van Noort D, Chiam K-H, Park S. 2013. *Sci. Rep.* 3:3247
55. Ai B-Q, Chen Q-Y, He Y-F, Li F-G, Zhong W-R. 2013. *Phys. Rev. E* 88:062129
56. Wu JC, Chen Q, Wang R, Ai BQ. 2014. *J. Phys. A: Math. Theor.* 47:325001
57. Ai B-Q, Wu J-C. 2014. *J. Chem. Phys.* 140:094103
58. Reichhardt C, Reichhardt CJO. 2013. *Phys. Rev. E* 88:062310
59. Kulic IM, Mani M, Mohrbach H, Thaokar R, Mahadevan L. 2009. *Proc. R. Soc. B* 276:2243–47
60. Pototsky A, Hahn AM, Stark H. 2013. *Phys. Rev. E* 87:042124
61. Stenhammar J, Wittkowski R, Marenduzzo D, Cates ME. 2016. *Sci. Adv.* 2(4):e1501850
62. Nikola N, Solon AP, Kafri Y, Kardar M, Tailleur J, Voituriez R. 2016. *Phys. Rev. Lett.* 117:098001
63. Weitz S, Blanco S, Fournier R, Gautrais J, Jost C, Theraulaz G. 2014. *Phys. Rev. E* 89:052715
64. Wu J-C, Chen Q, Wang R, Ai B-Q. 2015. *Physica A* 428:273–78
65. Mijalkov M, McDaniel A, Wehr J, Volpe G. 2016. *Phys. Rev. X* 6:011008
66. Drocco JA, Reichhardt CJO, Reichhardt C. 2012. *Phys. Rev. E* 85:056102
67. Mahmud G, Campbell CJ, Bishop KJM, Komarova YA, Chaga O, et al. 2009. *Nat. Phys.* 5:606–12
68. Sun X, Driscoll MK, Guven C, Das S, Parent CA, et al. 2015. *PNAS* 112:12557–62
69. Ghosh PK, Misko VR, Marchesoni F, Nori F. 2013. *Phys. Rev. Lett.* 110:268301
70. Koumakis N, Lepore A, Maggi C, Di Leonardo R. 2013. *Nat. Commun.* 4:2588
71. Lambert G, Liao D, Austin RH. 2010. *Phys. Rev. Lett.* 104:168102
72. Reichhardt C, Reichhardt CJO. 2014. *Phys. Rev. E* 90:012701
73. Maass CC, Krüger C, Herminghaus S, Bahr C. 2016. *Annu. Rev. Condens. Matter Phys.* 7:171–93
74. Wan M-B, Jho Y-S. 2013. *Soft Matter* 9:3255–61
75. Narayan V, Ramaswamy S, Menon N. 2007. *Science* 317:105–8
76. Sanchez T, Chen DTN, DeCamp SJ, Heymann M, Dogic Z. 2012. *Nature* 491:431–34

77. Giomi L, Bowick MJ, Ma X, Marchetti MC. 2013. *Phys. Rev. Lett.* 110:228101
78. DeCamp SJ, Redner GS, Baskaran A, Hagan MF, Dogic Z. 2015. *Nat. Mater.* 14:1110–15
79. DiLuzio WR, Turner L, Mayer M, Garstecki P, Weibel DB, et al. 2005. *Nature* 435:1271–74
80. Riedel IH, Kruse K, Howard J. 2005. *Science* 309:300–3
81. Li G, Tam L-K, Tang JX. 2008. *PNAS* 105:18355–59
82. Tierno P, Johansen TH, Fischer TM. 2007. *Phys. Rev. Lett.* 99:038303
83. Kümmel F, ten Hagen B, Wittkowski R, Buttinoni I, Eichhorn R, et al. 2013. *Phys. Rev. Lett.* 110:198302
84. ten Hagen B, Kümmel F, Wittkowski R, Takagi D, Löwen H, Bechinger C. 2014. *Nat. Commun.* 5:4829
85. Reichhardt C, Reichhardt CJO. 2003. *Phys. Rev. E* 68:046102
86. Speer D, Eichhorn R, Reimann P. 2009. *Phys. Rev. Lett.* 102:124101
87. Tierno P, Johansen TH, Fischer TM. 2007. *Phys. Rev. Lett.* 99:038303
88. Nourhani A, Crespi VH, Lammert PE. 2015. *Phys. Rev. Lett.* 115:118101
89. Reichhardt C, Reichhardt CJO. 2013. *Phys. Rev. E* 88:042306
90. Mijalkova M, Volpe G. 2013. *Soft Matter* 9:6376–81
91. Ai B, He Y, Zhong W. 2015. *Soft Matter* 11:3852–59
92. Ai B. 2016. *Sci. Rep.* 6:18740
93. Angelani L, Di Leonardo R, Ruocco G. 2009. *Phys. Rev. Lett.* 102:048104
94. Di Leonardo R, Angelani L, Dell'Arciprete D, Ruocco G, Iebba V, et al. 2010. *PNAS* 107:9541–45
95. Sokolov A, Apodaca MM, Grzyboswki BA, Aranson IS. 2010. *PNAS* 107:969–74
96. Kojima M, Miyamoto T, Nakajima M, Homma M, Arai T, Fukuda T. 2016. *Sens. Actuators B* 222:1220–25
97. Li H, Zhang HP. 2013. *Europhys. Lett.* 102:50007
98. Angelani L, Di Leonardo R. 2010. *New J. Phys.* 12:113017
99. Kaiser A, Peshkov A, Sokolov A, ten Hagen B, Löwen H, Aranson IS. 2014. *Phys. Rev. Lett.* 112:158101
100. Mallory SA, Valeriani C, Cacciuto A. 2014. *Phys. Rev. E* 90:032309
101. Kaiser A, Wensink HH, Löwen H. 2012. *Phys. Rev. Lett.* 108:268307
102. Kaiser A, Popowa K, Wensink HH, Löwen H. 2013. *Phys. Rev. E* 88:022311